



# Experimental investigation on effective aerosol scavenging using different spray configurations with pre-injection of water mist for Fukushima Daiichi decommissioning

Rui-Cong Xu<sup>1</sup> · Avadhesh Kumar Sharma<sup>2</sup> · Erdal Ozdemir<sup>2</sup> · Shuichiro Miwa<sup>1,2</sup> · Shunichi Suzuki<sup>1</sup>

Received: 1 July 2023 / Revised: 11 August 2023 / Accepted: 5 September 2023 / Published online: 9 April 2024  
© The Author(s) 2024

## Abstract

During the decommissioning of the Fukushima Daiichi nuclear power plant, it is important to consider the retrieval of resolidified debris both in air and underwater configurations. For the subsequent retrieval of debris from the reactor building, the resolidified debris must be cut into smaller pieces using various cutting methods. During the cutting process, aerosol particles are expected to be generated at the submicron scale. It has been noted that such aerosols sizing within the Greenfield gap (0.1–1  $\mu\text{m}$ ) are difficult to remove effectively using traditional spraying methods. Therefore, to improve the aerosol removal efficiency of the spray system, a new aerosol agglomeration method was recently proposed, which involves injecting water mist to enlarge the sizes of the aerosol particles before removing them using water sprays. In this study, a series of experiments were performed to clarify the proper spray configurations for effective aerosol scavenging and to improve the performance of the water mist. The experimental results showed that the spray flow rate and droplet characteristics are important factors for the aerosol-scavenging efficiency and performance of the water mist. The results obtained from this study will be helpful for the optimization of the spray system design for effective aerosol scavenging during the decommissioning of the Fukushima Daiichi plant.

**Keywords** Fukushima Daiichi decommissioning · Aerosol scavenging · Multiphase flow · Spray system · Aerosol-mist agglomeration

---

This work was financially supported by the Nuclear Energy Science and Technology and Human Resource Development Project of the Japan Atomic Energy Agency/Collaborative Laboratories for Advanced Decommissioning Science (No. R04I034). Ruicong Xu appreciates the scholarship (financial support) from the Chinese Scholarship Council (CSC No. 202106380073).

- 
- ✉ Rui-Cong Xu  
xurc@g.ecc.u-tokyo.ac.jp
  - ✉ Avadhesh Kumar Sharma  
avdhruva@gmail.com
  - ✉ Shuichiro Miwa  
miwa@n.t.u-tokyo.ac.jp

<sup>1</sup> Department of Nuclear Engineering and Management, The University of Tokyo, 7-3-1 Hongo, Bunkyo-Ku, Tokyo 113-8656, Japan

<sup>2</sup> Nuclear Professional School, The University of Tokyo, 2-22 Shirane-Shirakata, Tokai-Mura, Ibaraki 319-1188, Japan

## 1 Introduction

In the 2011 Fukushima Daiichi accident, radioactive reactor fuel was relocated and resolidified at the bottom of the reactor pressure vessel and primary containment vessel (PCV) due to the melting of the reactor core. During the decommissioning of the Fukushima Daiichi nuclear power plant (NPP), it is important to retrieve solid debris from damaged reactor buildings [1]. Prior to retrieval, debris and contaminated structural components should be cut using appropriate available techniques, such as laser cleaning and cutting [2, 3]. However, based on the initial laser cutting experiments conducted by Institut de Radioprotection et de Sûreté Nucléaire using debris simulants, it has been determined that the in- and ex-vessel laser cutting processes may generate the aerosol particles with mass median diameters of 0.27 and 0.16  $\mu\text{m}$ , respectively [4–6]. Moreover, the vibrations resulting from laser cleaning or cutting may potentially resuspend radioactive particles present on structural surfaces. Consequently, these radioactive aerosol particles of submicron size

have the potential to disperse into the atmosphere of PCVs, thereby posing radiological hazards to both the surrounding environment and general public.

To remove the aerosol particles in light water reactors (LWRs), different safety systems can be considered, such as filtered containment venting systems [7, 8], suppression pool scrubbing systems [9, 10], and containment spray systems [11]. However, in the case of severe LWR accidents, there is a risk of radioactive aerosol release due to filter and pool bypass [12]. Additionally, it is anticipated that the cutting and cleaning processes involved in the decommissioning of reactor components will likely result in the generation of aerosols. Considering the removal of radioactive aerosol particles inside the damaged PCVs after a severe LWR accident, the spray system is the most applicable and effective option for mitigating the aerosol suspensions inside a closed space and cooling the high-temperature debris with decay heat. As shown in Fig. 1, spray droplets can capture submicron aerosols through mechanical effects (including Brownian diffusion, interception, and inertial impaction), phoretic effects (that is, diffusiophoresis and thermophoresis), and electroscavenging [13, 14]. To study water spray for washing out aerosol particles in the case of severe NPP accidents and decommissioning, some experimental studies have been conducted, such as those at the TOSQAN facility [11, 15], SCRUPOS facility [16], and COSTTHES facility [17]. However, it has been noted that the aerosols within the Greenfield gap (0.1–1  $\mu\text{m}$ ) [18], which specifically pose significant concerns in case of Fukushima Daiichi, are difficult to be effectively removed by the spray droplets because of the low collection efficiency. Considering the Fukushima Daiichi decommissioning task, it is of significant importance to improve the scavenging efficiency of aerosol particles in the Greenfield

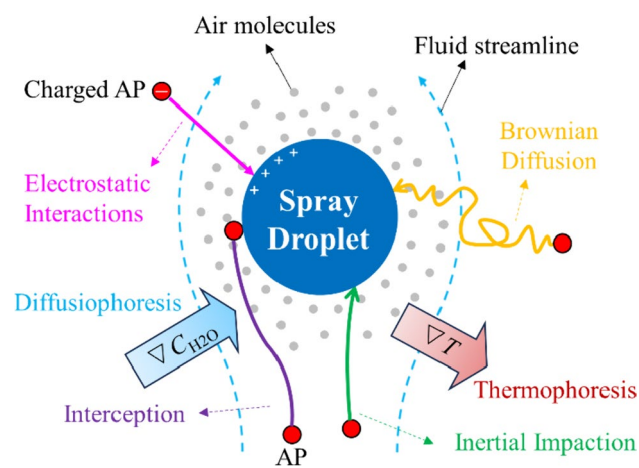


**Fig. 1** (Color online) Illustration of mechanisms of aerosol collection by a downward falling spray droplet. Abbreviation: aerosol particle (AP)

gap for better mitigation of fission products and less contaminated water production.

Therefore, to improve the aerosol removal efficiency of the spray system, a new aerosol agglomeration method was recently proposed by injecting water mist to increase the sizes of aerosol particles before removing them using water sprays [19–21]. As illustrated in Fig. 2, Greenfield aerosols are expected to coalesce with water mist particles, forming larger agglomerated particle clusters comprising aerosol particles and water mist. According to the experiments performed at the University of Tokyo, Aerosol Removal Tests facility with Sprays (UTARTS) [19–21], it was confirmed that the pre-injection of water mist can significantly improve the aerosol spray scavenging efficiency by increasing the size of aerosols. However, it should be highlighted that the different spray configurations (for example, spray angle, spray flow rate, etc.) along with different spray droplets characteristics (for example, droplet size distribution, droplet velocity, etc.) may play an essential role on the performance of the enlarged aerosol-mist particles in improving the aerosol removal efficiency. Therefore, it is important to study effective aerosol scavenging under different spray and mist configurations for the optimization of the spray system for Fukushima Daiichi decommissioning.

Motivated by the objective of enhancing the understanding of aerosol scavenging, achieving improved mitigation of fission products, and reducing the production of contaminated water during the decommissioning of the Fukushima Daiichi NPP, we conducted a comprehensive series of experiments in this study employing different spray nozzles and concentrations of the injected water mist to examine the effectiveness in aerosol scavenging. Section 2 provides an overview of the experimental conditions and procedures. Section 3 presents the experimental results and corresponding analyzes. The conclusions and potential future directions are outlined in Sect. 4. It is anticipated that the results of this study will contribute to the optimization of spray system designs for efficient aerosol scavenging during the decommissioning process at Fukushima Daiichi.

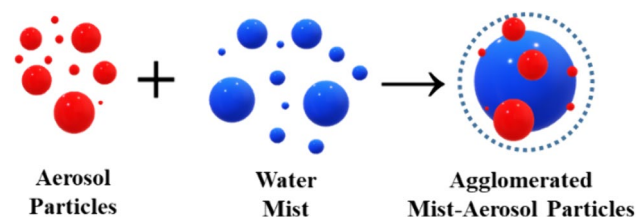


**Fig. 2** (Color online) Agglomeration method for aerosol particles using water mist

## 2 Experimental conditions

### 2.1 Experimental setup

Figure 3 shows a schematic of the UTARTS experimental system. The main experimental facility was a stainless-steel containment vessel 2.5-m in height, 1.5-m in diameter, and 3.92-m<sup>3</sup> in volume. Thirteen optical observation windows and one manhole were installed on the facility wall for visualization inside the vessel. Several small holes were inserted into the sidewalls of the facility for mist injection and measurements using the aerosol sampling line. A water discharge hole was used to control the valve

at the central bottom of the vessel. A spray injection tube was inserted through the flange at the center of the top of the vessel. A hole near the spray nozzle entrance flange was used to discharge aerosol particles with gas outside the facility after the experiments. The discharged gas was filtered using a high-efficiency particulate air (HEPA) filter before being exhausted.

In this study, four spray nozzles fabricated by a spraying system company were employed. The nozzle scheme is illustrated in Fig. 3, and Table 1 lists the important nozzle parameters. As listed in Table 1, Nozzles 1, 2, and 3 are single-hole full-cone nozzles with different spray configurations and droplet characteristics. However, considering that the washing space of single-hole nozzles is insufficient for

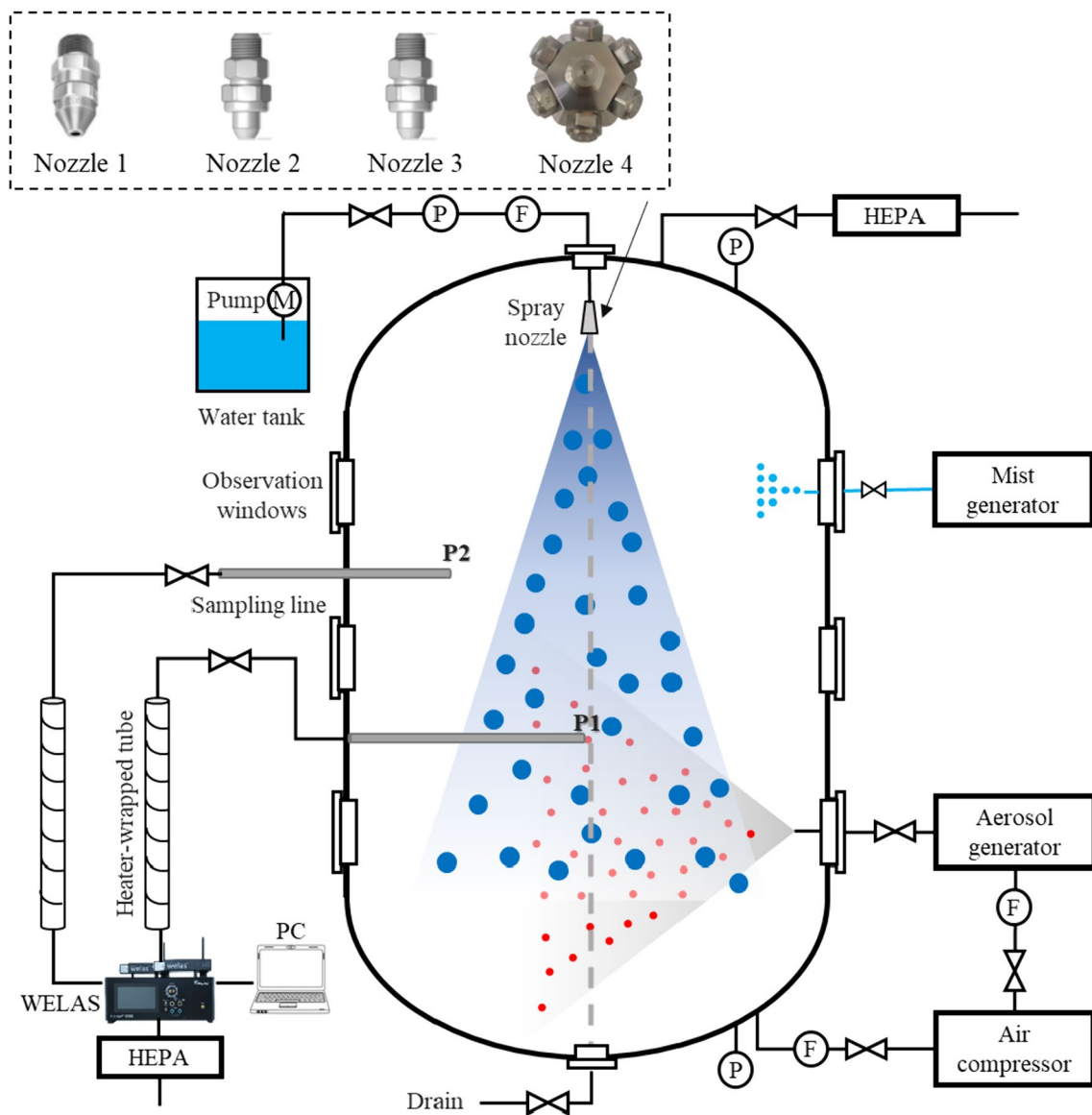


Fig. 3 (Color online) Schematic of the UTARTS facility

**Table 1** Parameters of the spray nozzles used in the experiments

Nozzle number	1	2	3	4
Model	GG-30	TG-3.5	TG2	FORJET 1-7 N SS BSPT
Number of nozzle hole	1	1	1	7
Orifice diameter (mm)	1.2	1.7	1.2	1.1 for each orifice
Spray angle <sup>a</sup> (°)	26–32	46–50	46–50	120~162
Average droplet velocity magnitude at 2 L/min <sup>b</sup> (m/s)	20	–	18	7
Average droplet velocity magnitude at 3 L/min <sup>b</sup> (m/s)	32	15	30	9
Average droplet velocity magnitude at 4 L/min <sup>b</sup> (m/s)	–	–	–	12
Droplet Sauter mean diameter (μm)	309	344	302	162
Spray pattern of the whole nozzle	Full cone	Full cone	Full cone	Full cone
Distance from the top of vessel (cm)	30	30	30	35

<sup>a</sup>The data of spray angles were provided by the manufacturer

<sup>b</sup>The average droplet velocities were measured near the nozzle outlets by using the PIV (Particle Image Velocimetry) and Shadowgraphy techniques [20, 21, 23]. The velocity of droplets will gradually decrease during their falling

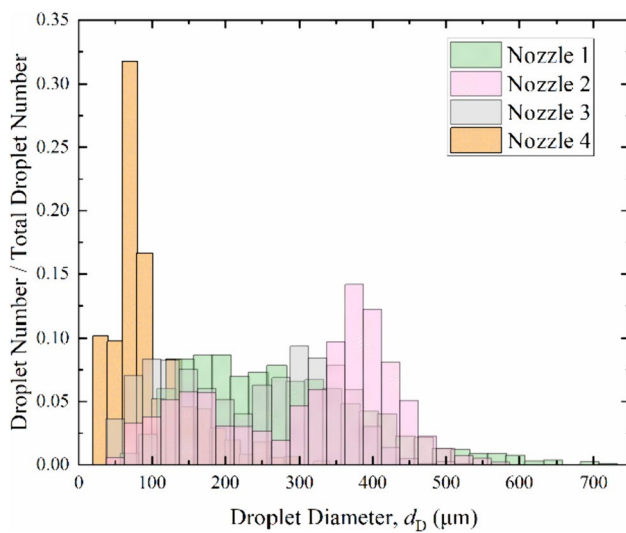


**Fig. 4** (Color online) Droplet size distributions from different spray nozzles

large-scale Fukushima PCVs, a spray system with multiple nozzles or outlets is suggested for actual Fukushima Dai-ichi decommissioning [22]. Thus, a multi-orifice Nozzle 4 comprising seven orifices with one at the center and six at the sides, as shown in Fig. 3, was utilized to increase the washing space. The spray droplet size distributions of the nozzles are shown in Fig. 4. The droplet size distributions were determined by the shadowgraphy and interferometric laser imaging for droplet sizing techniques [20, 23]. Figure 5 schematically illustrates the spray patterns of the nozzles. During the experiments, spray water was injected into a water tank using a pump. Aerosol particles of  $ZrO_2$  with a mass median diameter  $d_{50}=0.15\ \mu\text{m}$  were employed to simulate particles from laser cutting of fuel debris.  $ZrO_2$  aerosol particles are considered because according to the laser cutting tests on in- and ex-vessel fuel debris simulants, a large proportion of  $ZrO_2$  particles with mass mean diameters of  $0.16\ \mu\text{m}$  and  $0.27\ \mu\text{m}$  were found to be generated [3].

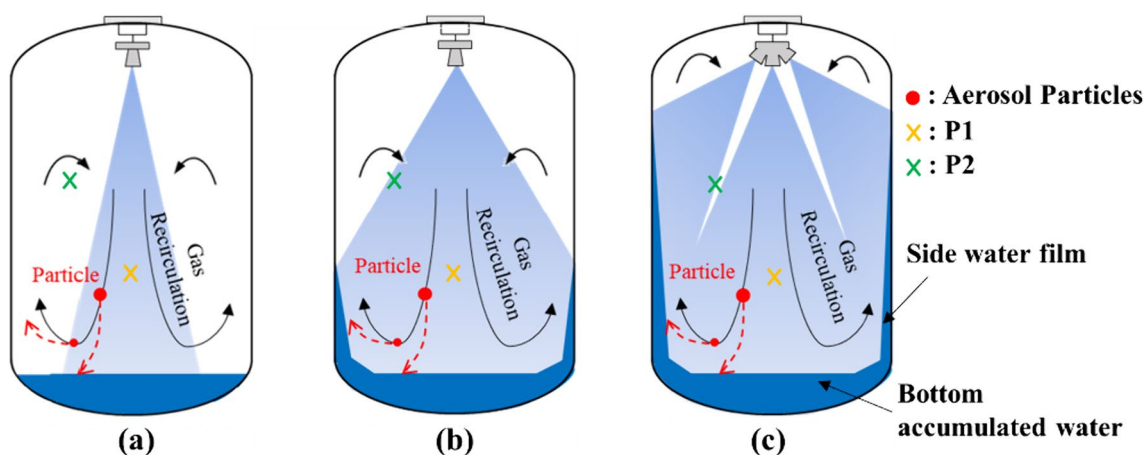


**Fig. 5** (Color online) Schematic of gas recirculation, accumulated water and water film: **a** Nozzle 1; **b** Nozzles 2 and 3; **c** Nozzle 4

Before the experiments, dry  $ZrO_2$  particles inside the generator chamber were blown via high-pressure airflow injection through a Laskin nozzle and turbulence due to fan rotation. The aerosol particles were then injected into the vessel.

An ultrasonic mist generator (MZ-JH30, Japan Yamazen Company) was used for submicron water mist generation and injection. For the aerosol measurement, two points are considered: one measurement point (P1) was on the half diameter of the vessel and 1.4-m below the nozzle outlet, while the other (P2) was 0.4-m from the vessel sidewalls and 0.85-m below the nozzle outlet. The aerosol sampling line was used to measure the aerosol concentrations at different positions. In the experiments, both sampling lines were used to evaluate the variations in aerosol concentrations. To eliminate water mist in the sampling flows before entering the aerosol analyzer, heater-wrapped tubes of 1.2-mm in length were installed before the aerosol analyzer, which could be heated up to  $180^\circ C$ . After passing through the heater-wrapped tubes, the aerosol sample flows entered the aerosol analyzer Welas3000, where the aerosol particle number concentration and size distribution during the experiments were measured. Welas3000 is a light-scattering spectrometer system that can measure particle concentrations from  $< 1$  particle/cm<sup>3</sup> to  $10^6$  particle/cm<sup>3</sup> and particle sizes ranging from 0.2 to  $10\ \mu m$  with an absolute measurement error of  $\pm 0.01\ \mu m$  and relative error of 5% [24].

## 2.2 Experimental procedures

The general experimental procedure is illustrated in Fig. 6. First, aerosol particles were generated and injected into the vessel until the particle concentration reached the target value. Then, the bottom blowing gas was performed for 15 min to ensure that the aerosol particles were uniformly dispersed inside the vessel. In the experiments using water mist, the mist was injected by the humidifier and dispersed inside the vessel for 15 min. The initial setting of the humidifier was varied to achieve different concentrations of water mist. In this study, a mist with a low concentration was achieved by initially adjusting the humidifier to the lowest setting, whereas a high concentration was achieved using the highest setting. After mist injection, the experiment was performed for another 15 min to provide sufficient time for the aerosol mist agglomeration so that larger-sized coagulated aerosol-mist particles could be formed. The spray injection was then activated continuously for 60 min to remove aerosol particles and water mist. During spray activation, aerosol concentrations at different points were measured using the aerosol analyzer Welas 3000. After completing the measurement, the spray was deactivated, and the accumulated

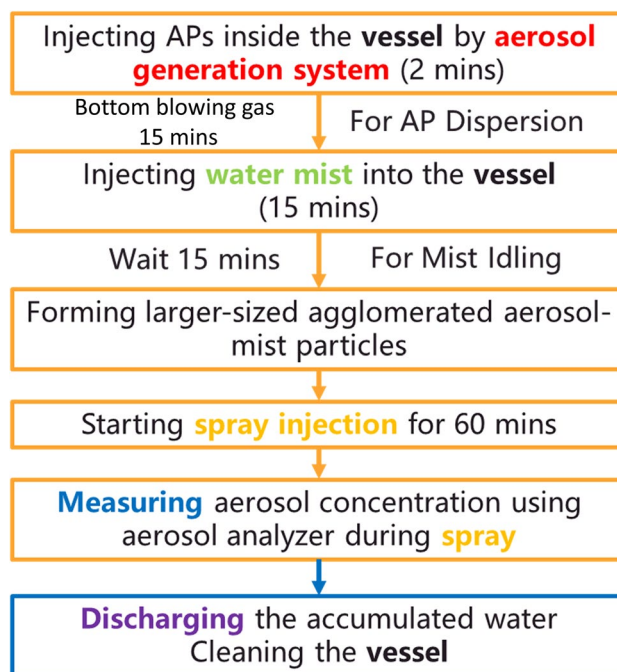


Fig. 6 Experimental procedures. Abbreviation: aerosol particle (AP)

spray water in the lower part of the vessel was discharged. Simultaneously, the remaining aerosol-containing gas was exhausted using a HEPA filter. The main door in the vessel was then opened to clean the interior.

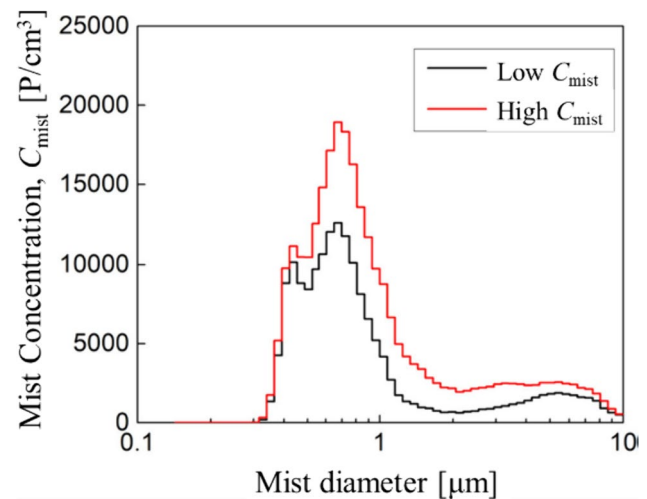
## 2.3 Experimental cases

Thirty-two experiments were conducted to investigate effective aerosol scavenging using different spray configurations with water mist for Fukushima Daiichi decommissioning. Table 2 lists the experimental conditions for each case. The experiments were performed at room temperature ( $\sim 20^\circ C$ ) and atmospheric pressure ( $\sim 1$  bar). The spray water and mist were collected at room temperature. Three different mist concentrations ( $C_{mist}$ ) (no mist, low  $C_{mist}$ , and high  $C_{mist}$ ) were used to investigate the effects of water mist on aerosol scavenging. Figure 7 illustrates the mist concentration levels and size distributions for both low- and high-concentration mists. For both mist concentration levels, the mist size was distributed around similar peaks with a diameter of  $0.68\ \mu m$ . In our previous study [19], by calculating the collection kernels of different mechanisms for mist-aerosol coagulation under several reasonable assumptions, it was verified that under our experimental conditions, the contribution of the mechanisms to mist-aerosol coagulation can be

**Table 2** Experimental cases

Case number	Nozzle number	Spray flow rate, $Q$ (L/min)	Mist concentration, $C_{mist}$
1	1	2.0	No mist
2			Low $C_{mist}$
3			High $C_{mist}$
4		2.4	No mist
5			High $C_{mist}$
6		3.0	No mist
7			High $C_{mist}$
8	2	2.0	No mist
9			Low $C_{mist}$
10			High $C_{mist}$
11		2.4	No mist
12			High $C_{mist}$
13		3.0	No mist
14			High $C_{mist}$
15		4.0	No mist
16			High $C_{mist}$
17	3	2.0	No mist
18			Low $C_{mist}$
19			High $C_{mist}$
20		2.4	No mist
21			High $C_{mist}$
22		3.0	No mist
23			High $C_{mist}$
24	4	2.0	No mist
25			Low $C_{mist}$
26			High $C_{mist}$
27		2.4	No mist
28			High $C_{mist}$
29		3.0	No mist
30			High $C_{mist}$
31		4.0	No mist
32			High $C_{mist}$

ranked by: (1) gravitational coagulation, (2) Brownian coagulation, (3) turbulent shear-induced coagulation, (4) laminar shear-induced coagulation, and (5) turbulent inertial coagulation. Additionally, the effect of water mist on increasing the aerosol size was verified by comparing the aerosol concentration probability density function before and after mist injection and idling [21]. In addition to the mist concentration, the spray nozzle and spray flow rate ( $Q$ ) were also considered as experimental parameters to understand the influence of spray configurations on aerosol scavenging.

**Fig. 7** Mist size distribution for low and high concentration levels [19]

## 3 Results and discussion

### 3.1 Aerosol size distribution variation during spray

Figure 8 shows the variations in the aerosol size distribution of the aerosol number and mass concentrations during the 3 L/min spray from Nozzle 4 without mist injection. The variations in the aerosol mass concentration shown in Fig. 8b were estimated by assuming spherical shaped aerosol particles. The black line in Fig. 8 shows the initial size distribution before spraying, whereas the other lines show the experimental data obtained at 1, 3, 5, 10, 20, 30, 40, 50, and 60 min. It can be observed that the aerosol number concentration peaks appear at 0.55  $\mu\text{m}$ . Although the number concentration of the submicron particles was larger than that of the micron-sized particles, the mass concentration of the micron-sized particles was larger because of the heavier weight of the particles. Both the number and mean mass diameters were larger than the initial median mass diameter of the aerosol particles. This indicates that aerosol particles can agglomerate, as confirmed by scanning electron microscopy analysis [25]. Here, it is worthwhile to note that according to our previous experimental measurement [19], the relative humidity inside the UTARTS chamber increases from environmental humidity (approximately 65%) to 99% after the 400-second spray due to the generated small droplets. The falling time of the droplet inside the chamber was short because of its high velocity compared to the chamber scale. Thus, the effect of diffusiophoresis on the capture of aerosol particles surrounding falling spray droplets can be

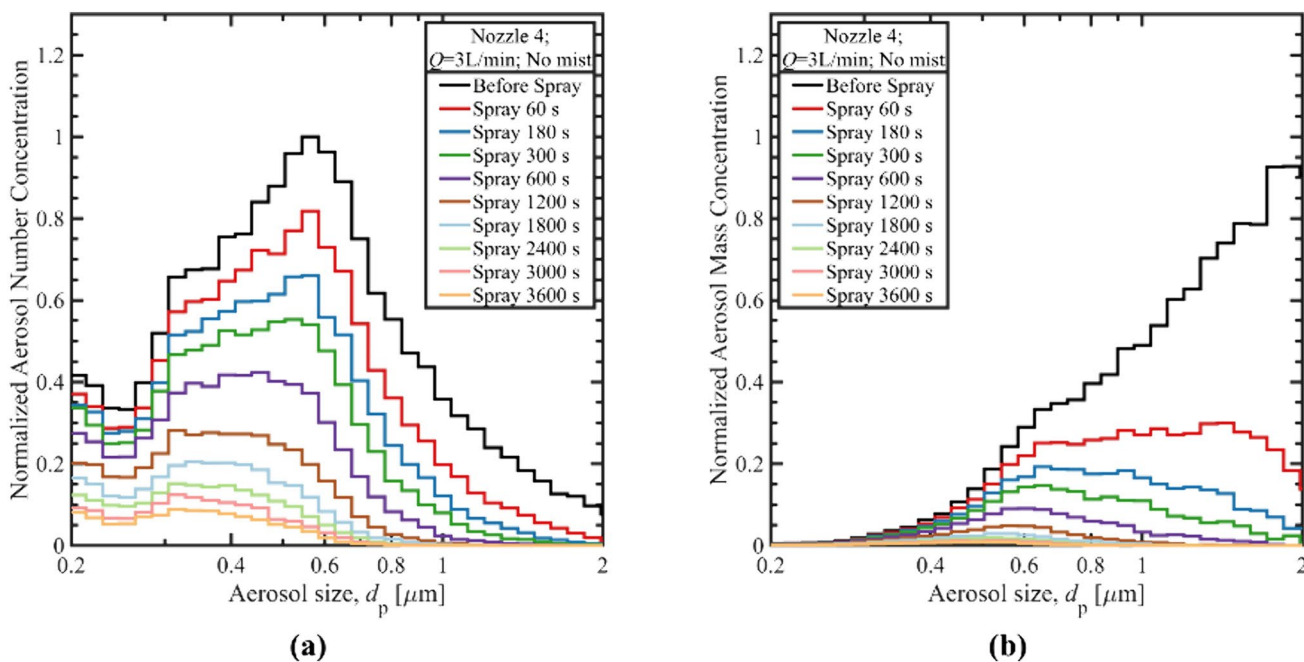


**Fig. 8** (Color online) Aerosol size distribution variation during spray (Case 29: Nozzle 4;  $Q=3\text{L}/\text{min}$ ; No mist): **a** Normalized aerosol number concentration, **b** Normalized aerosol mass concentration

neglected in comparison with other effects (for example, initial impaction, interception, and Brownian diffusion). Furthermore, during spray activation, the concentration of larger aerosol particles reduced faster than that of smaller particles, especially for the mass concentration variation depicted in Fig. 8b. As shown in Fig. 8, after a 60-min spray, the larger aerosol particles were almost completely removed, whereas the smaller particles (especially those smaller than  $0.4\ \mu\text{m}$ ) still remained, leading to a reduction in the concentration peak. This obvious variation in the aerosol size distribution can be attributed to the fact that compared to the smaller aerosol particles, the larger particles can be removed more effectively due to the more significant inertial impaction and interception from the spray droplets.

### 3.2 Aerosol scavenging efficiency and removal rate

To evaluate the scavenging efficiency of aerosol particles of varying sizes under different spray configurations and mist concentrations, the scavenging efficiency after  $t_{\text{spray}}$  spray time for a certain aerosol size was defined according to the ratio of the difference in the number concentration of aerosol particles,  $C_n(t)$ , between  $t=0\ \text{s}$  and  $t=t_{\text{spray}}$  to the concentration at  $t=0\ \text{s}$ :

$$E(t_{\text{spray}}) \Big|_{d=d_p} = \frac{C_n(0\text{s}) \Big|_{d=d_p} - C_n(t_{\text{spray}}) \Big|_{d=d_p}}{C_n(0\text{s}) \Big|_{d=d_p}} \tag{1}$$

Additionally, to assess the aerosol removal rates during the entire spray process, the balance equation for the variation in aerosol particle concentration in the gas space of the vessel during spraying was considered [11]:

$$\frac{dC_n(t_{\text{spray}})}{dt} = -\lambda_s C_n(t_{\text{spray}}) + S_{\text{source}} + S_{\text{deposition}} \tag{2}$$

where  $\lambda_s$  is the aerosol removal rate during the entire scavenging process by water spray;  $S_{\text{source}}$  and  $S_{\text{deposition}}$  represent the aerosol source and loss terms, respectively.

In this study,  $S_{\text{source}}$  and  $S_{\text{deposition}}$  were both assumed to be zero, because there was no further aerosol injection into the vessel once the spray was activated and the aerosol particle deposition rate was negligible compared to that from spray scavenging. Hence, the following expression can be derived from Eq. (2):

$$C_n(t_{\text{spray}}) = C_n(0\text{s})e^{-\lambda_s t_{\text{spray}}} \tag{3}$$

In this study, the data of aerosol number concentration during 60–1200 s spray were considered for the data fitting to determine the value of  $\lambda_s$  in general. However, for those cases with very fast aerosol removal (such as Case 16 with high spray flow rate and high mist concentration), the data of aerosol number concentration during 60 s to the time before 99% aerosol particles being removed are selected to ensure the accurate determination of  $\lambda_s$ .

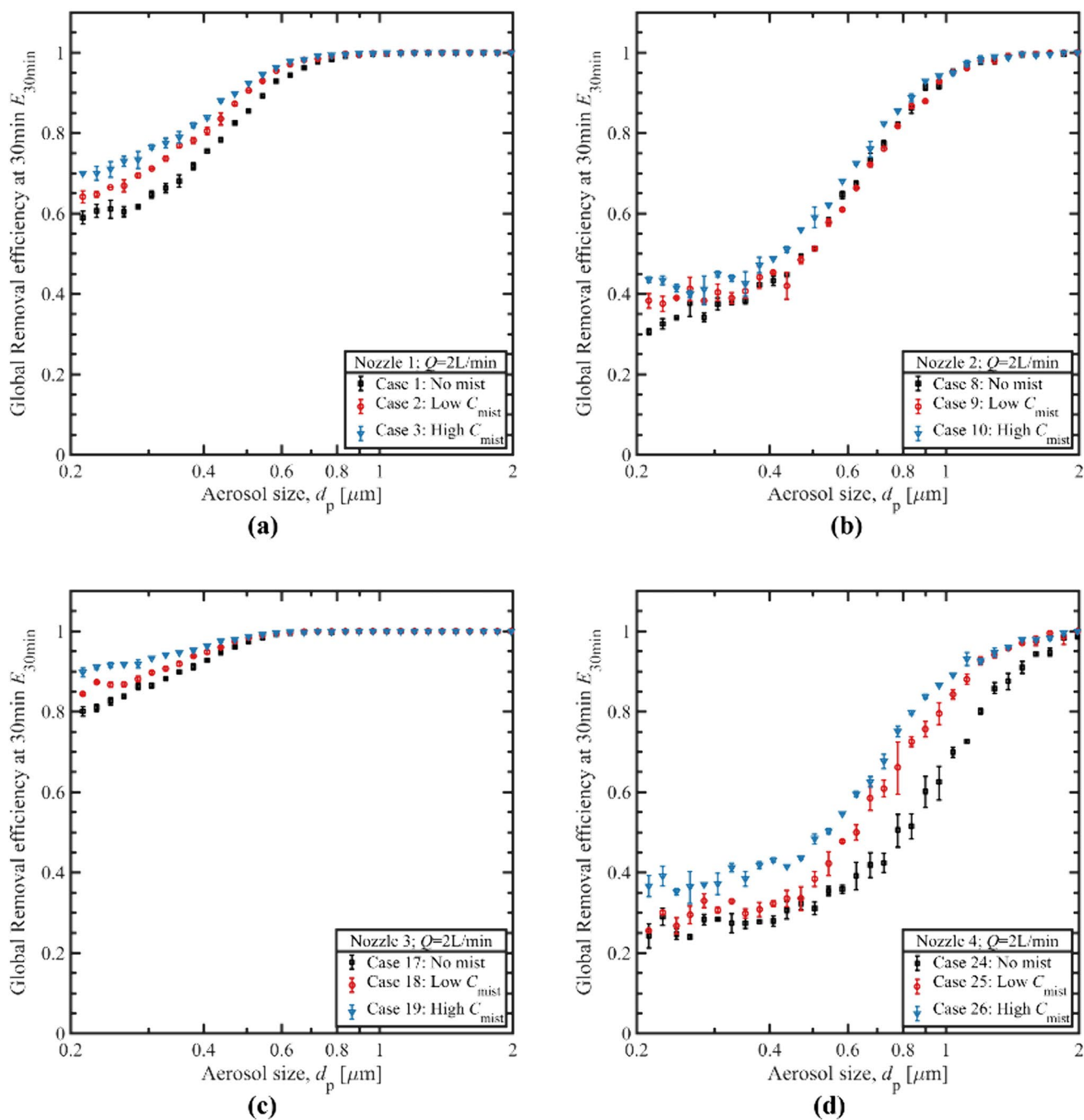


**Fig. 9** (Color online) Comparisons of aerosol scavenging efficiencies at different mist concentrations after 30-min spray ( $Q=2\text{L}/\text{min}$ ): **a** Nozzle 1, **b** Nozzle 2, **c** Nozzle 3, **d** Nozzle 4

### 3.3 Effect of mist

Figure 9 shows the aerosol-scavenging efficiency  $E$  at 30-min 2 L/min spray. The error bars in each case represent the standard deviations of  $E$  values following the different measurement points. From Fig. 7, it can be observed that

irrespective of the spray nozzles, the aerosol scavenging efficiencies can be increased due to the injection of water mist for all aerosol particles of different sizes. Furthermore, a larger mist concentration promoted aerosol scavenging efficiencies more significantly, especially for those inside the Greenfield gap. This phenomenon can be understood as

follows. In the presence of water mist, the diffusiophoresis mechanism compels the aerosol particles within the experimental chamber to migrate toward the water mist surface. Additionally, mist-aerosol coagulation may also occur due to different mechanisms, especially gravitational coagulation and Brownian coagulation [19]. Additionally, it is plausible that the surface wettability of aerosol particles is enhanced by their agglomeration with the mist, resulting in improved hydrophilicity. Consequently, these agglomerated particles exhibited an increased affinity toward the spray droplets, facilitating their removal. The aerosol-scavenging efficiency was enhanced in cases where mist injection was employed, primarily because of the enlargement of aerosol particles and the resulting improvement in hydrophilicity.

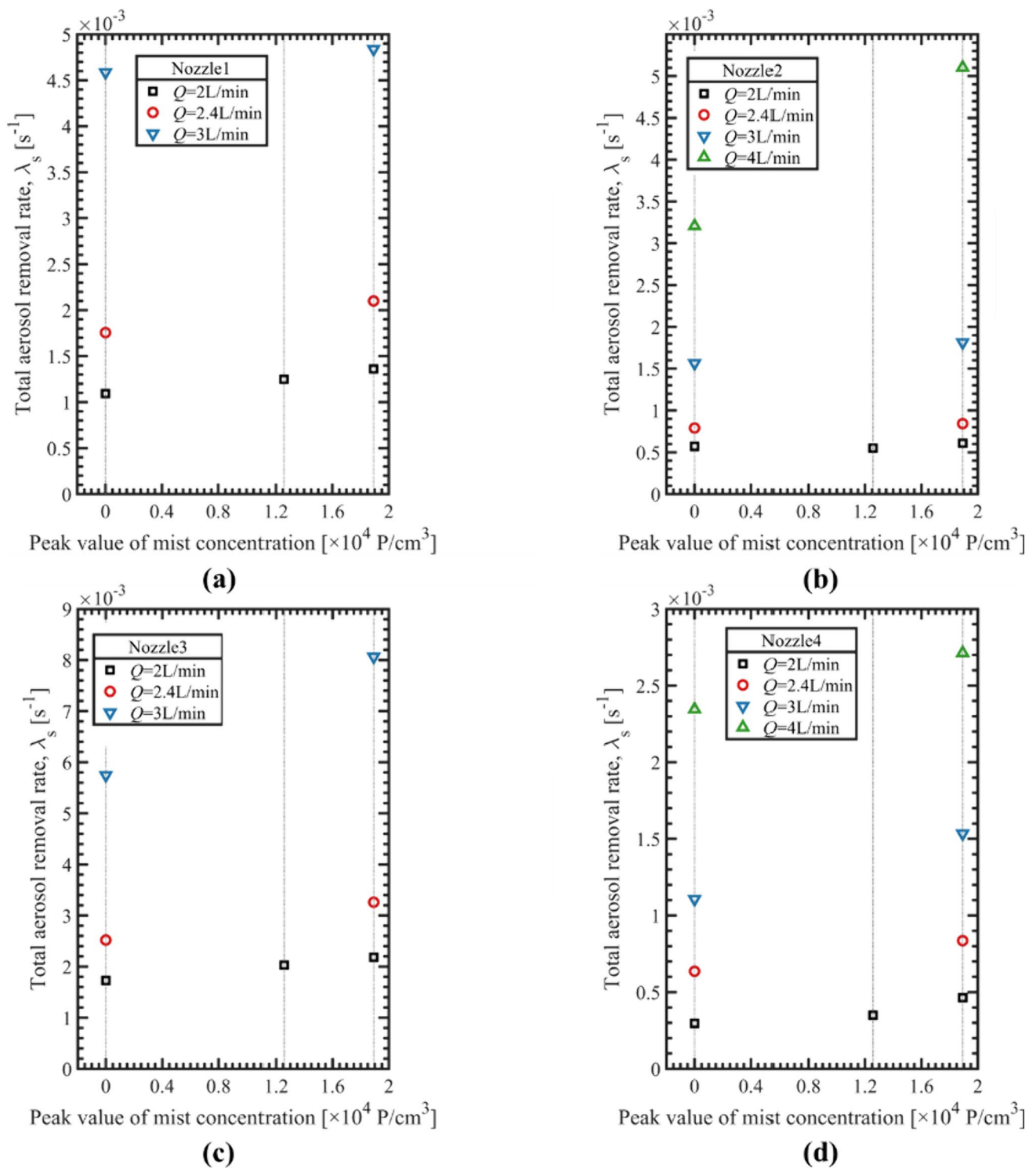
Moreover, a comparison of Fig. 9b with Fig. 9a, c, and d shows that the enhancement of the aerosol scavenging efficiency is less pronounced when Nozzle 2 is utilized. This observation indicates that the configuration of the spray nozzle may also impact the efficacy of the water mist in improving the aerosol scavenging efficiency. Specifically, for the 2 L/min spray using Nozzle 2, the water mist is found to be more effective in improving the scavenging efficiency for smaller aerosol particles (for example,  $d_p < 0.4 \mu\text{m}$ ) in general. This is because of the enhanced diffusiophoresis and improved surface wettability of the aerosol-mist agglomerated particles. However, for larger aerosol particles, the aerosol scavenging efficiency slightly improved when using a high-concentration mist. When using a low-concentration mist, the scavenging efficiency of the larger-sized aerosol particles seemed to be similar to that of the neutral spray condition, with a very slight deviation. Notice that the droplet velocity for Nozzle 2 is slower and the mist also promotes aerosol-mist agglomeration to enlarge the sizes of aerosol particles. This may be because in the case of low flow rates, the inertial impaction, which is effective in capturing larger aerosol particles, has a less significant contribution to the aerosol collections due to the lower droplet velocity, leading to a smaller improvement in the total collection efficiency. Furthermore, the contribution of the droplet velocity in enhancing the aerosol scavenging efficiency also explains why the scavenging efficiencies were different for Nozzles 2 and 3, although both nozzles shared similar cone angles and droplet size distributions.

Figure 10 shows the aerosol removal rates at different mist concentrations for different spray nozzles. This figure clearly confirms that the aerosol removal rates can be improved by adding water mist, irrespective of the spray configuration. However, different spray configurations can affect the performance of the water mist in improving the aerosol removal rate. For example, according to Fig. 10a–d, increasing the spray flow rate aids in improving the performance of the

water mist (especially for Nozzles 2 and 3), indicating that the different characteristics of spray droplets are essential in removing aerosol-mist agglomerated particles via different collection mechanisms. The differences in the droplet velocity, which can not only influence the inertial aerosol capture, but also the gas entrainment to the spray region, may also significantly affect the performance of the water mist, according to the comparison between the results from Nozzles 2 and 3. In the following subsections, the effects of spray configurations on the aerosol scavenging efficiency and performance of water mist are discussed in more detail based on the evaluation of the aerosol collection efficiencies of different mechanisms by droplets.

### 3.4 Evaluation of aerosol collection efficiencies

As described above, spray droplets can capture aerosol particles through mechanical effects (including Brownian diffusion, interception, and inertial impaction), phoretic effects (that is, diffusiophoresis and thermophoresis), and electro-scavenging [13, 14]. It should be noted here that considering the aerosol collection mechanisms by spray droplets in the present study, inertial impaction, interception, and Brownian diffusion play more significant roles in removing aerosol particles than diffusiophoresis and thermophoresis [17, 26], and electro-scavenging is not considered in this study. Table 3 summarizes the models for aerosol collection efficiency using a single spray droplet. Based on the information of droplet characteristics (including droplet size distribution and average droplet velocity) in Table 2 and the models listed in Table 3, the average collection efficiencies of aerosol particles ranging from 0.2 to 1  $\mu\text{m}$  in size by a single droplet from different nozzles at 3 L/min spray are evaluated, as shown in Fig. 11. The average collection efficiencies are obtained by calculating the collection efficiencies for the single droplet for possible sizes and assuming that the droplet-driven particle-laden gas velocity magnitude is negligible in the comparison with that of the droplets under the experimental conditions. From Fig. 11, it can be observed that the collection efficiencies of the inertial impaction by a single droplet for Nozzles 1 and 3 are generally comparable and larger than those for Nozzles 2 and 4, respectively, owing to their larger droplet velocities. Nozzle 4 exhibited the largest collection efficiencies of interception and Brownian diffusion because of its finer droplet size. However, from Figs. 11a–c, it can be observed that inertial impaction plays a dominant role in aerosol collection by a single droplet compared to interception and Brownian diffusion. Therefore, as shown in Fig. 11d, the relationship governing total aerosol collection efficiency by a single droplet between the four



**Fig. 10** (Color online) Aerosol removal rates at different mist concentrations: **a** Nozzle 1, **b** Nozzle 2, **c** Nozzle 3, **d** Nozzle 4

nozzles is generally:  $\eta_{\text{total, nozzle1}} \approx \eta_{\text{total, nozzle3}} > \eta_{\text{total, nozzle2}} > \eta_{\text{total, nozzle4}}$ .

Figure 12 shows the average total collection efficiencies of a single droplet for the Nozzle-4 spray at different flow rates. It is observed that increasing the spray flow rates is

**Table 3** Models for aerosol collection efficiency by a single droplet [27, 28]

Aerosol collection mechanism	Model of aerosol collection efficiency by a single droplet
Inertial impaction, $\eta_{imp}^a$	$\eta_{imp} = \begin{cases} 0, & St \leq 0.083 \\ 8.57 \times \left(\frac{St}{St+0.5}\right)^2 \times (St - 0.083), & 0.083 < St < 0.2 \\ \left(\frac{St}{St+0.5}\right)^2, & St \geq 0.2 \end{cases}$ <p>with</p> $St = \frac{\rho_p d_p^2  U_G - U_D }{9 \mu_G d_D}$
Interception, $\eta_{int}^b$	$\eta_{int} = \frac{1 - \alpha_L}{J + \sigma \cdot K} \left\{ \left(\frac{R}{1+R}\right) + \frac{1}{2} \left(\frac{R}{1+R}\right)^2 \cdot (3\sigma + 4) \right\}$ <p>with</p> $R = \frac{d_p}{d_D}, J = 1 - \frac{6}{5} \cdot \alpha_L^{\frac{1}{3}} + \frac{1}{5} \cdot \alpha_L^2, K = 1 - \frac{9}{5} \cdot \alpha_L^{\frac{1}{3}} + \frac{1}{5} \cdot \alpha_L^2$
Brownian diffusion, $\eta_{diff}^c$	$\eta_{diff} = (2 \times Pe \times d_D)^{-\frac{1}{2}}$ <p>with</p> $Pe = \frac{d_D  U_G - U_D }{D_{diff}}, D_{diff} = \frac{k_B T C}{3 \pi v_G \rho_G d_p}, C = \frac{2.609 \sqrt{2l}}{\sqrt{d_p}}$
Total collection efficiency, $\eta_{total}$	$\eta_{total} = 1 - (1 - \eta_{imp})(1 - \eta_{int})(1 - \eta_{diff})$

<sup>a</sup>In the model for the inertial impaction, *St* is the Stokes number;  $\rho_p$  is aerosol particle density;  $d_p$  and  $d_D$  mean aerosol particle diameter and spray droplet diameter, respectively;  $U_G$  and  $U_D$  signify the velocity of gas and droplet, respectively;  $\mu_G$  is the dynamic viscosity of air

<sup>b</sup>In the model for the interception, *J* and *K* are two empirical factors related to the volume fraction of liquid phase  $\alpha_L$ ;  $\sigma$  stands for the ratio of dynamic viscosities between spray droplets and gas phase; *R* represents the ratio of diameters between the aerosol particles and the water droplets

<sup>c</sup>In the model for the Brownian diffusion, *Pe* is Peclet number;  $D_{diff}$  represents the diffusion coefficient; *C* is the Cunningham correction factor;  $k_B$  is Boltzmann constant;  $v_G$  is the kinematic viscosity of air gas; *T* is temperature; *l* signifies the mean free path length of air

effective for increasing the total aerosol collection efficiency by a single droplet. This is because a higher spray flow rate enhanced the production of droplets with higher velocities. High-velocity droplets have sufficient inertia to ensure that more aerosol particles do not follow their original streamline around the spray droplets and move sufficiently close to the droplet surfaces, leading to collisions. However, collection by Brownian diffusion is restricted to a certain degree. Based on this understanding of the aerosol collection efficiencies of a single droplet, the effects of the spray flow rate and nozzle are analyzed in the following subsections.

### 3.5 Effect of spray flow rate

Figure 13 shows the effect of the spray flow rate on the aerosol scavenging efficiencies after different spray times for Nozzles 1 and 4 under the no-mist and high-mist conditions. It can be seen that regardless of the spray nozzle, the aerosol scavenging efficiencies can be significantly increased with a higher flow rate. This is more evident at the earlier spray stage where the aerosol particles are not completely removed at high spray flow rates (for example, the 10-min spray shown in Fig. 13a and b). This is because not only

can the total aerosol collection efficiency be improved by a larger spray flow rate due to the enhanced predominance and collection efficiency of inertial impaction, as shown in Fig. 12, but also because denser droplets facilitate faster aerosol removal. The high-velocity droplets had sufficient inertia to ensure that more aerosol particles did not follow their original streamline around the spray droplets and moved sufficiently close to the droplet surface, leading to collisions. Additionally, spray droplets with higher velocities may promote gas recirculation from the peripheries to the center of the experimental vessel [29], as shown in Fig. 5. Thus, smaller gas-containing aerosol particles, which move more easily following the gas streamlines, may move from the periphery toward the center and re-enter the spray region, thereby improving the overall scavenging efficiency. This effect is expected to be more significant if the nozzle has a smaller spray angle (for example, Nozzle 1 shown in Fig. 5a), which means that the spray droplets are concentrated within the center of the vessel. From Fig. 13, it can be seen that the aerosol scavenging efficiencies at a specific spray time can be improved more significantly by employing both a higher spray flow rate and higher concentration of mist.

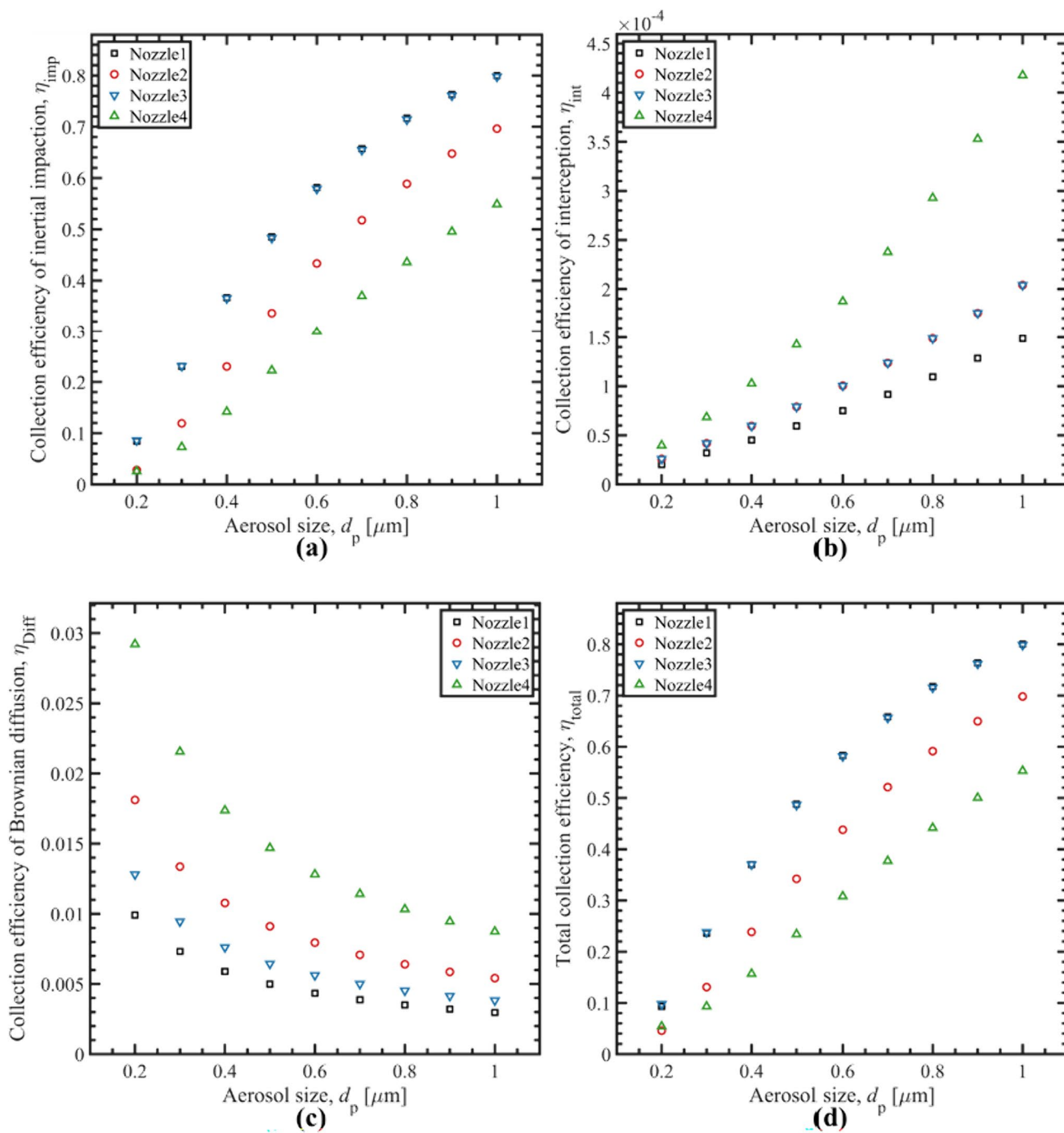


**Fig. 11** Evaluation of average collection efficiencies of aerosol particles in the Greenfield gap by a single droplet from different nozzles under 3 L/min spray: **a** Collection efficiency of inertial impac-

tion, **b** Collection efficiency of interception, **c** Collection efficiency of Brownian diffusion, **d** Total collection efficiency

However, considering the decommissioning of Fukushima Daiichi NPP, one important issue is the reduction of contaminated water production. The aerosol scavenging efficiencies for different spray flow rates and mist concentrations

under the same water consumption (120 L) are compared in Fig. 14. It can be seen in the figure that by increasing the spray flow rate with the same water consumption, more

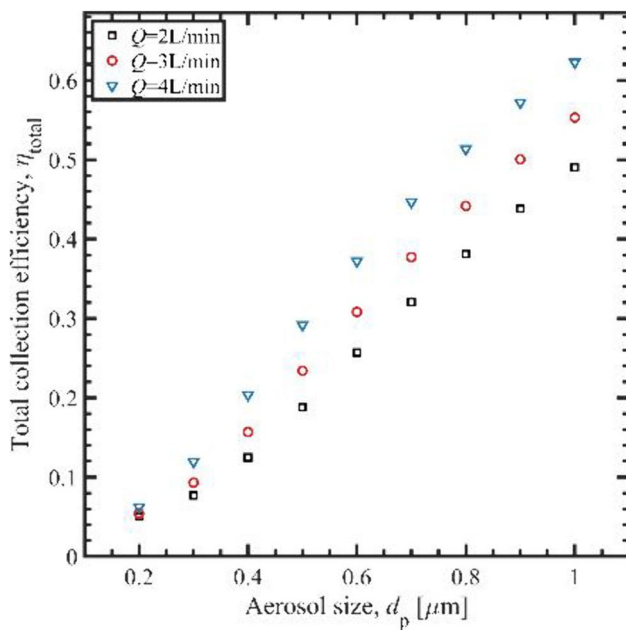


**Fig. 12** Average total collection efficiencies by a single droplet for Nozzle-4 spray at different flow rates

aerosol particles can be captured by the spray droplets owing to their higher velocity to promote the collection of inertial impaction and enhance the reentry of the aerosol particles to the center. The effect of the mist on improving the aerosol scavenging efficiency can be confirmed by comparing Fig. 14a, c, b, and d. Therefore, to better mitigate fission products and reduce contaminated water production during Fukushima Daiichi decommissioning, it is suggested to utilize higher spray flow rates and higher concentrations of injected water mist, based on the results of the current study.

Moreover, to investigate the effect of the spray flow rate on the performance of water mist in improving the aerosol removal rates, Fig. 15 shows the aerosol removal rates for different nozzles at different spray flow rates for all nozzles considered in the current experiments. In this figure, the solid and dashed lines show the data at the “No mist” and “High  $C_{\text{mist}}$ ” conditions, respectively; and the data from the same nozzle are shown in the same color and point style. From Fig. 15, it is seen that the performance of the mist in improving the aerosol removal rates is generally optimized when a higher spray flow rate is used. This may be because in the case of high flow rates, the inertial impaction, which is more effective for capturing larger-sized aerosol particles, has a more significant contribution to the collections of larger-sized aerosol-mist agglomerates owing to the high droplet velocity, leading to a higher total collection efficiency (for example, the examples shown in Fig. 12). The

performance of the water mist was less evident for Nozzles 2 and 4 at low spray flow rates, which may be due to the smaller increase in the aerosol collection efficiency with an increase in the aerosol particle size. Another important observation in Fig. 15 is that for Nozzle 1, increasing the spray flow rate has a less significant effect on the performance of the water mist. This may be explained by the fact that the spray angle of Nozzle 1 was smaller than those of the other nozzles, as shown in Table 2. In this case, re-entrainment of gas-containing aerosol particles to the central spray region is essential for aerosol capture by the droplets. However, enlarged aerosol particles with larger Stokes numbers make it difficult to direct the recirculating gas streamlines toward the center of the vessel, resulting in less improvement in the mist performance in aerosol scavenging.

### 3.6 Effect of spray nozzle

To further study the effects of the spray configuration and droplet characteristics on aerosol scavenging, the aerosol scavenging efficiencies for different spray nozzles after 30-min spray are compared in Fig. 16. The figure shows that regardless of the spray flow rate and mist concentration, the aerosol scavenging efficiency has the following relationship:  $E_{\text{Nozzle3}} > E_{\text{Nozzle1}} > E_{\text{Nozzle2}} > E_{\text{Nozzle4}}$ . The relationship of spray angles is:  $\theta_{\text{Nozzle4}} > \theta_{\text{Nozzle2}} \approx \theta_{\text{Nozzle3}} > \theta_{\text{Nozzle1}}$ , and simply increasing the spray space may not aid in improving the aerosol scavenging efficiency. The spray droplet characteristics (for example, velocity and size) may play more significant roles. From Table 2, the relationship of the droplet Sauter mean diameter from different nozzles is:  $d_{D,\text{Nozzle3}} > d_{D,\text{Nozzle1}} > d_{D,\text{Nozzle2}} > d_{D,\text{Nozzle4}}$ ; and the relationship of droplet velocities is:  $U_{D,\text{Nozzle1}} \approx U_{D,\text{Nozzle3}} > U_{D,\text{Nozzle2}} > U_{D,\text{Nozzle4}}$ . Comparing the data of Nozzles 1 and 3 shown in Fig. 16, Nozzle 3 shows larger aerosol scavenging efficiencies, although it is known that the average total aerosol collection efficiencies of a single droplet for Nozzles 1 and 3 are similar (see Fig. 11d), and  $U_{D,\text{Nozzle1}}$  are comparable with  $U_{D,\text{Nozzle3}}$ . One reason for this could be that the droplets of Nozzle 3 are smaller than those of Nozzle 1, and smaller droplets are produced by Nozzle 3, resulting in the production of denser droplets. This means that more droplets fell into the vessel during a unit time in the case of Nozzle 3. Additionally, as illustrated in Fig. 5a, the spray water can only accumulate at the bottom of the vessel if Nozzle 1 is employed, due to its smaller spray angle. However, in the case of Nozzle 3, water films may have formed at the side of the vessel (see Fig. 5b) due to its wider spray angle. When moving aerosol particles experience significant inertia, they can be captured by the surfaces of both the water films and

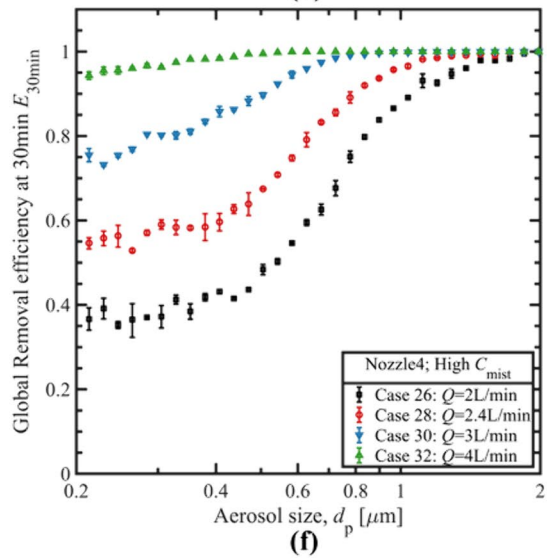
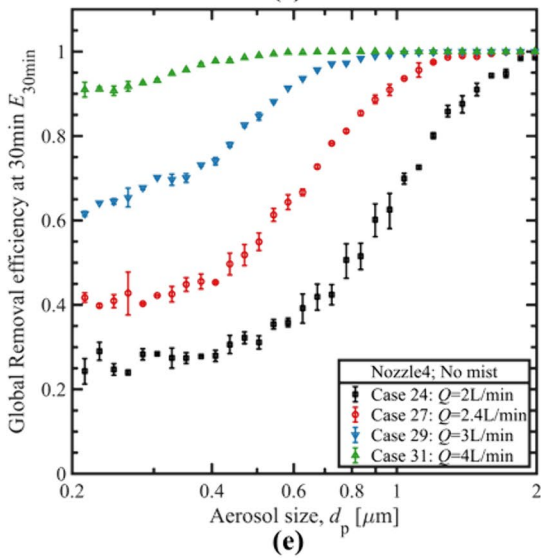
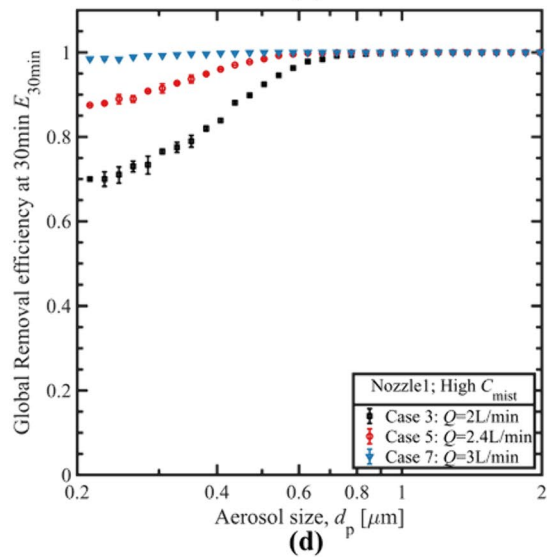
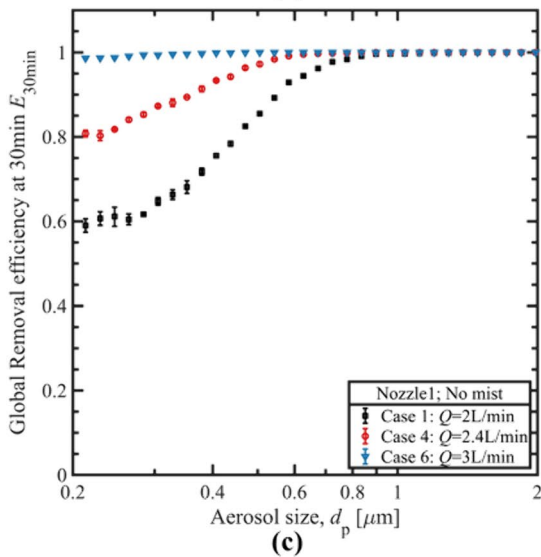
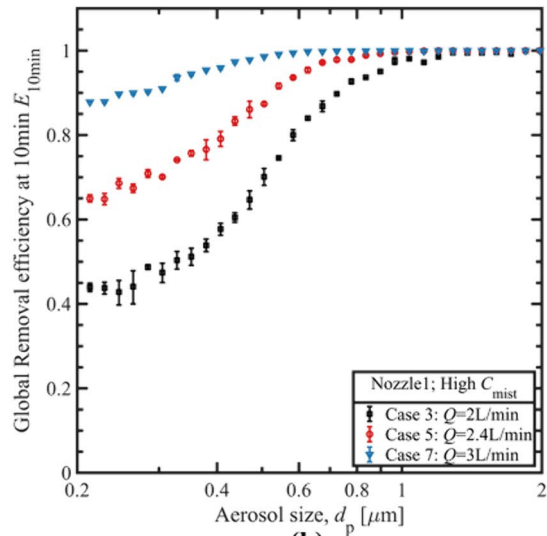
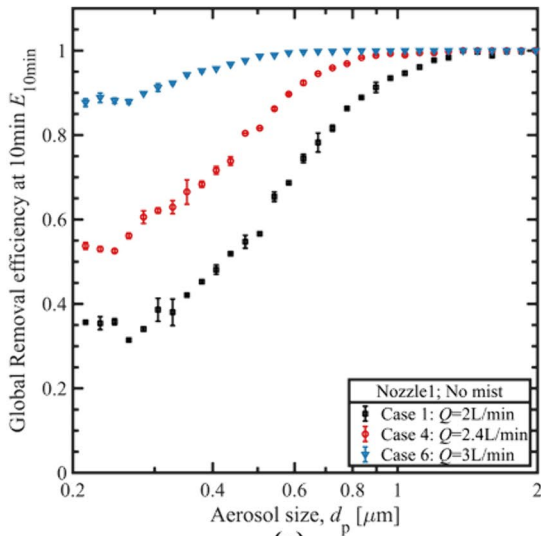


**Fig. 13** (Color online). Comparisons of aerosol scavenging efficiencies for different spray flow rates: **a** Nozzle 1 after 10-min spray (No mist), **b** Nozzle 1 after 10-min spray (High  $C_{mist}$ ), **c** Nozzle 1 after 30-min spray (No mist), **d** Nozzle 4 after 30-min spray (High  $C_{mist}$ ), **e** Nozzle 4 after 30-min spray (No mist), **f** Nozzle 4 after 30-min spray (High  $C_{mist}$ )

accumulated water. As a result, Nozzle 3 showed better aerosol scavenging than Nozzle 1.

Additionally, according to Fig. 16, Nozzle 4, which had the widest spray angles in the current study, showed the lowest aerosol scavenging efficiency despite the larger surface area of accumulated water. Water films formed during spraying and the densest droplets discharged into the vessel.

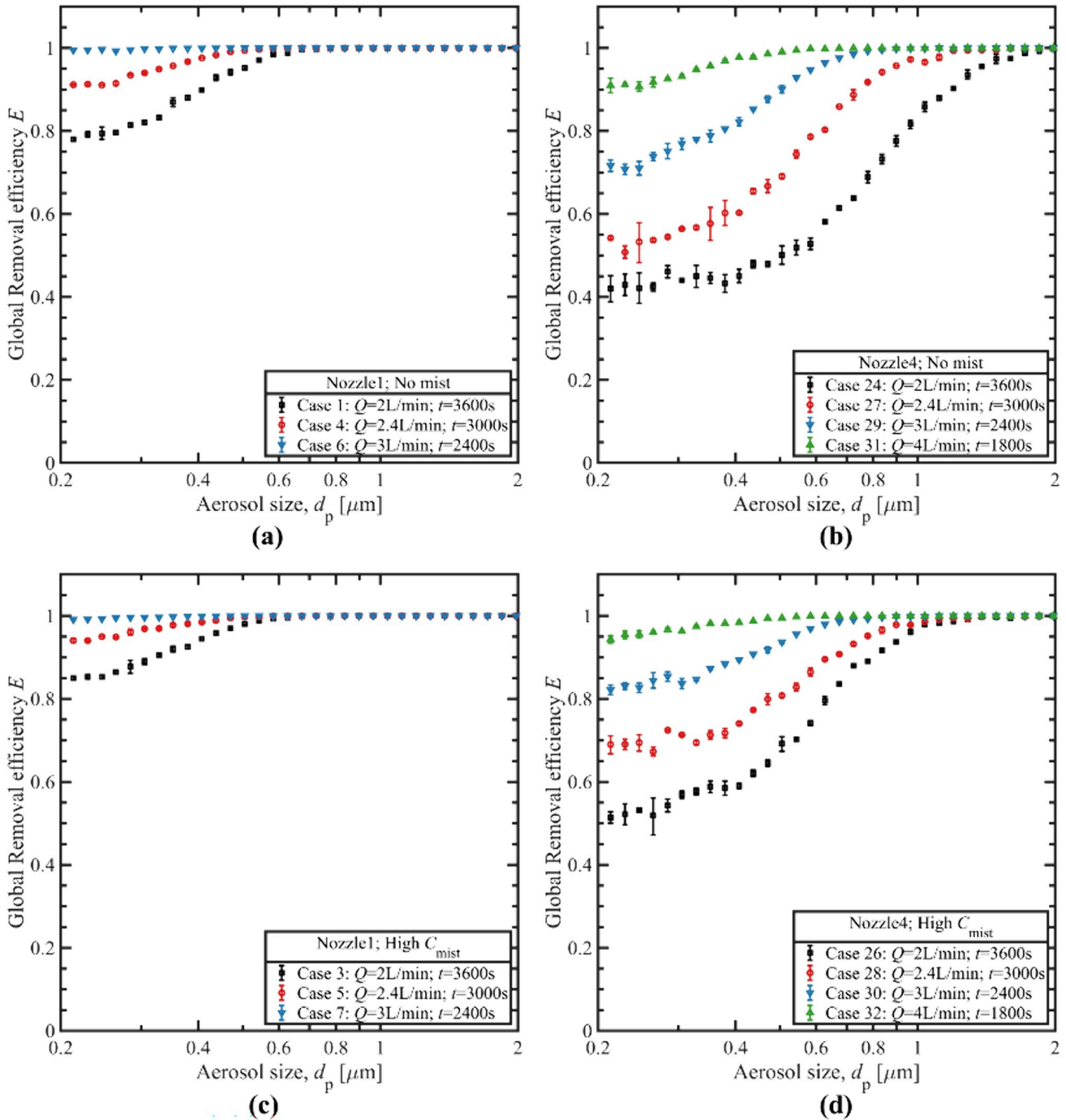


**Fig. 14** (Color online) Comparisons of aerosol scavenging efficiencies for different spray flow rates and mist concentrations under the same water consumptions (120 L): **a** Nozzle 1 (No mist), **b** Nozzle 4 (No mist), **c** Nozzle 1 (High  $C_{mist}$ ), **d** Nozzle 4 (High  $C_{mist}$ )

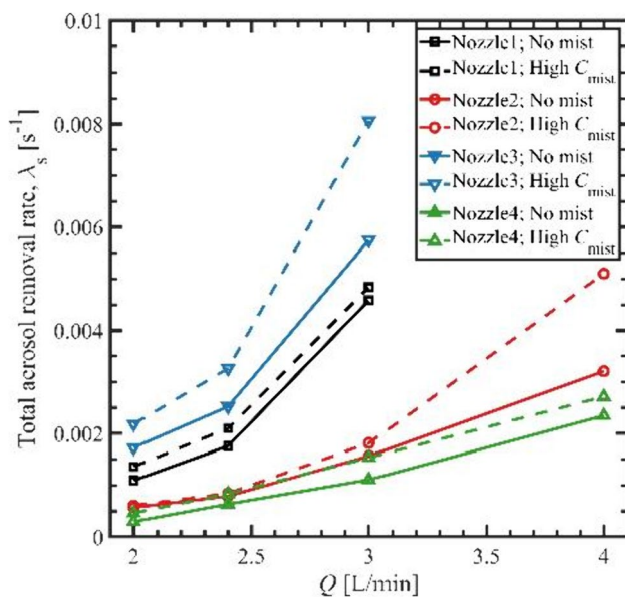


**Fig. 15** (Color online) Aerosol removal rates for different nozzles at different spray flow rates

From Fig. 11d, it can be seen that the average total aerosol collection efficiencies by a single droplet is generally the lowest, although the value for 0.2- $\mu\text{m}$  aerosol particles is slightly higher than that of Nozzle 2. Another reason why the aerosol scavenging efficiency of Nozzle 4 is the lowest is that the volume of droplets passing through the aerosol-containing gas is smaller during unit time due to the low droplet velocities; thus, the overall removed aerosol particles are relatively limited.

The effect of the spray nozzle on the performance of the water mist in improving the aerosol removal rate can be understood from Fig. 15. As described in Sect. 3.5, the smaller improvement in the aerosol collection efficiency with increasing aerosol particle size may be the reason for the lower performance of the water mist for Nozzles 2 and 4 at low flow rates. However, with an increase in the flow rate (for example, 4 L/min), the improvement in the water mist performance for Nozzle 2 was more significant than that of Nozzle 4. This may have resulted from the larger increase in velocity for Nozzle 2, which promoted a significant improvement in the aerosol collection efficiency for enlarged aerosol particles. When comparing the data displayed in Fig. 15 for Nozzles 1 and 3, which produced spray droplets with similar velocities, the improvement in the mist performance for Nozzle 3 was more evident. One possible reason is that the aerosol particles enlarged by water mist are more difficult to

direct along gas recirculation streamlines toward the spray center in case of Nozzle 1 with a narrow spray angle. Additionally, it can be seen that the aerosol-mist agglomerated particles not only enlarge the aerosol sizes, but also improve the hydrophilicity of aerosols. Hence, the larger surface area of the accumulated water and water films in the case of Nozzle 3 can capture more aerosol particles during spraying. Therefore, considering aerosol spray scavenging for Fukushima Daiichi decommissioning, widening the spray angle should not be adopted at the expense of the spray droplet velocity. It is suggested that the spray system be designed with a wider spray angle and the high-velocity droplets with proper size distributions be adopted to improve the performance of the water mist and aerosol scavenging efficiency.

## 4 Conclusion

In this study, we conducted an experimental investigation to evaluate the effectiveness of aerosol scavenging by utilizing an appropriate spray system with pre-injection of water mist. Various spray configurations combined with the pre-injection of water mist were employed within the UTARTS facility for this purpose. The experimental results validate the effect of water mist on improving the aerosol removal efficiency owing to aerosol-mist agglomeration. It was also confirmed that increasing the spray flow rate can improve the aerosol scavenging efficiency with less water consumption because of the higher aerosol collection efficiency of droplets, denser droplets sprayed, and more significant gas recirculation to drive small aerosols to the spray region. Additionally, a wider spray angle can form a larger surface of accumulated water and water films at the bottom and side of the vessel, enhancing the capture of moving aerosol particles with strong inertia (for example, large aerosol particles).

Further, it was found that the spray configuration and droplet characteristics are important factors influencing the performance of water mist in improving the aerosol removal rate. Generally, the water mist performance can be optimized if a higher spray flow rate is used because of the higher aerosol collection efficiency of the enlarged aerosol particles. However, increasing the spray flow rate may also increase the Stokes number of the enlarged aerosol-mist agglomerated particles, making it difficult to follow the recirculating gas streamline to the center region, thereby restraining the mist performance in the case of narrow-angle spray. Additionally, a wider spray angle helps broaden the surface of the accumulated water and water films to capture aerosol-mist agglomerated particles with higher wettability, thereby promoting the effect of the water mist. Considering the effective

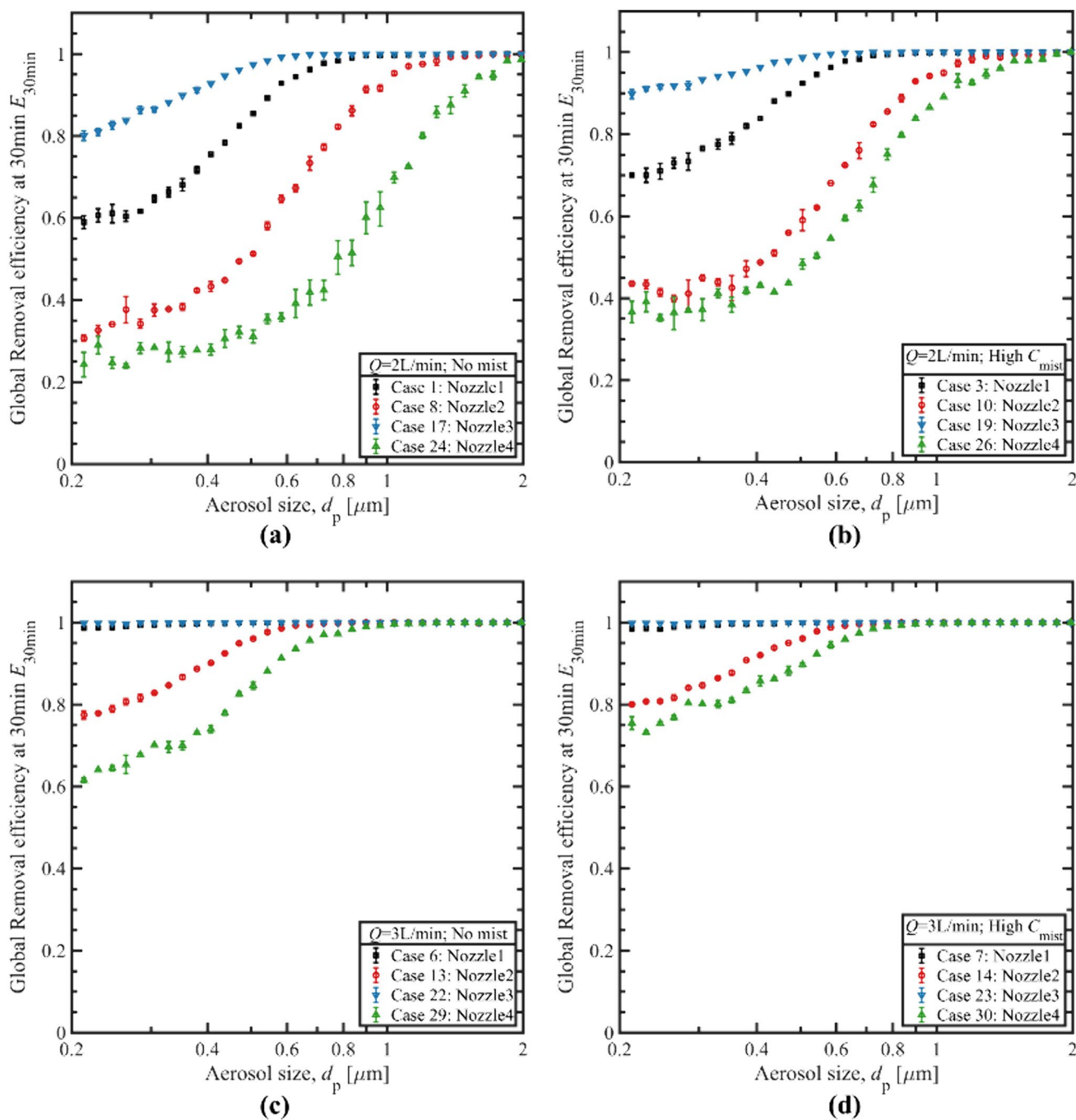


**Fig. 16** (Color online) Comparisons of aerosol scavenging efficiencies for different spray nozzles after 30-min spray: **a**  $Q=2L/min$  (No mist), **b**  $Q=2L/min$  (High  $C_{mist}$ ), **c**  $Q=3L/min$  (No mist), **d**  $Q=3L/min$  (High  $C_{mist}$ )

aerosol spray scavenging and high performance of the water mist for Fukushima Daiichi decommissioning, a spray nozzle capable of producing high-velocity droplets with proper

size distributions and a wider spray angle should be designed and utilized. Based on the current experimental results, an optimal combination of droplet size, discharge velocity,

spraying space, and mist concentration may be leveraged to achieve effective aerosol removal for a given system under a fixed spray water flow rate (or fixed consumption of water). The results obtained from the present study are expected to aid in optimizing the spray system design for effective aerosol scavenging during the Fukushima Daiichi decommissioning.

A proper design of the spray system is of significant importance for controlling radioactive aerosols and reducing contaminated water production during the Fukushima Daiichi decommissioning. To attain a better understanding of the spray system design, experiments using laser cleaning of debris simulant materials as an aerosol generation source together with different spray configurations at different locations in the UTARTS facility will be performed. Additionally, a more precise quantification of droplet characteristics, which is necessary for a more comprehensive evaluation and understanding of an efficient spray system design, will be performed in the near future. To further improve the aerosol-scavenging efficiency of the spray system, experiments with charging systems for spray droplets, water mist, and aerosol particles will be conducted in the future.

**Author contributions** All authors contributed to the conception and design of this study. Material preparation, data collection, and analysis were performed by RX, AKS, EO and SM. The first draft of the manuscript was written by RX and all authors commented on previous versions of the manuscript. All authors read and approved the final manuscript.

**Funding** Open Access funding provided by The University of Tokyo.

**Data availability statement** The data that support the findings of this study are openly available in Science Data Bank at <https://cstr.cn/31253.11.sciencedb.10101> and <https://doi.org/10.57760/sciencedb.10101>.

## Declarations

**Conflict of interest** The authors declare that they have no competing interests.

**Open Access** This article is licensed under a Creative Commons Attribution 4.0 International License, which permits use, sharing, adaptation, distribution and reproduction in any medium or format, as long as you give appropriate credit to the original author(s) and the source, provide a link to the Creative Commons licence, and indicate if changes were made. The images or other third party material in this article are included in the article's Creative Commons licence, unless indicated otherwise in a credit line to the material. If material is not included in the article's Creative Commons licence and your intended use is not permitted by statutory regulation or exceeds the permitted use, you will need to obtain permission directly from the copyright holder. To view a copy of this licence, visit <http://creativecommons.org/licenses/by/4.0/>.

## References

1. Inter-Ministerial Council for Contaminated Water and Decommissioning Issues, Mid-and-Long-Term roadmap toward the decommissioning of TEPCO's Fukushima Daiichi nuclear power station (2019). [https://www.meti.go.jp/english/earthquake/nuclear/decommissioning/pdf/20191227\\_3.pdf](https://www.meti.go.jp/english/earthquake/nuclear/decommissioning/pdf/20191227_3.pdf)
2. A.K. Sharma, H. Liang, R.C. Xu et al., Radioactive aerosol control and decontamination in the decommissioning of the Fukushima Daiichi nuclear power station. *Nucl. Technol.* **209**, 2030–2043 (2023). <https://doi.org/10.1080/00295450.2023.2186675>
3. E. Porcheron, C. Dazon, T. Gelain et al., Fukushima Daiichi fuel debris retrieval: results of aerosol characterization during laser cutting of non-radioactive corium simulants. *J. Nucl. Sci. Technol.* **58**, 87–99 (2021). <https://doi.org/10.1080/00223131.2020.1806135>
4. C. Journeau, D. Roulet, E. Porcheron et al., Fukushima Daiichi fuel debris simulant materials for the development of cutting and collection technologies. *J. Nucl. Sci. Technol.* **55**, 985–995 (2018). <https://doi.org/10.1080/00223131.2018.1462267>
5. E. Porcheron, S. Peillon, T. Gelain et al., *Analysis of aerosol emission and dispersion during the laser cutting of Fukushima fuel debris simulants*, in *26th International Conference on Nuclear Engineering (ICONE 26)*, London, England, July 22–26 (2018). <https://doi.org/10.1115/ICONE26-81531>
6. E. Porcheron, Y. Leblois, T. Gelain et al., Assessment of spray and pool scrubbing efficiencies for means of mitigation against aerosol dispersion in the context of fuel debris retrieval at Fukushima Daiichi: part I. *J. Nucl. Eng. Radiat. Sci.* **8**, 031701 (2022). <https://doi.org/10.1115/1.4051611>
7. J. Yang, D.Y. Lee, S. Miwa et al., Overview of filtered containment venting system in nuclear power plants in Asia. *Ann. Nucl. Energy* **119**, 87–97 (2018). <https://doi.org/10.1016/j.anucene.2018.03.047>
8. Y.M. Zhou, Z.N. Sun, H.F. Gu et al., Development of structural optimization design method for multilayer metal fiber filter in nuclear power plant. *Prog. Nucl. Energy* **124**, 103361 (2020). <https://doi.org/10.1016/j.pnucene.2020.103361>
9. H. Diao, Y.M. Zhou, H.F. Gu et al., Experimental study on the scrubbing efficiency of aerosols contained in horizontal and vertically downward submerged gas jet. *Prog. Nucl. Energy* **126**, 103406 (2020). <https://doi.org/10.1016/j.pnucene.2020.103406>
10. M. Pellegrini, L. Araneo, H. Ninokata et al., Suppression pool testing at the SIET laboratory: experimental investigation of critical phenomena expected in the Fukushima Daiichi suppression chamber. *J. Nucl. Sci. Technol.* **53**, 614–629 (2016). <https://doi.org/10.1080/00223131.2015.1134359>
11. E. Porcheron, P. Lemaitre, D. Marchand et al., Experimental and numerical approaches of aerosol removal in spray conditions for containment application. *Nucl. Eng. Des.* **240**, 336–343 (2010). <https://doi.org/10.1016/j.nucengdes.2008.08.023>
12. B.R. Sehgal (ed.), *Nuclear Safety in Light Water Reactors: Severe Accident Phenomenology*, 1st edn. (Academic Press, Cambridge, 2012). <https://doi.org/10.1016/C2010-0-67817-5>
13. K.K. Murata, D.C. Williams, R.O. Griffith et al., *Code manual for CONTAIN 2.0: A computer code for nuclear reactor containment analysis*, NUREG/CR-6533, SAND-97-1735 (1997). <https://doi.org/10.2172/569132>
14. K. Ardon-Dryer, Y.W. Huang, D.J. Cziczko, Laboratory studies of collection efficiency of sub-micrometer aerosol particles by cloud droplets on a single-droplet basis. *Atmos. Chem. Phys.* **15**, 9159–9171 (2015). <https://doi.org/10.5194/acp-15-9159-2015>
15. E. Porcheron, Y. Leblois, T. Gelain et al., Assessment of spray and pool scrubbing efficiencies for means of mitigation against aerosol dispersion in the context of fuel debris retrieval at Fukushima

- Daiichi: Part II. *J. Nucl. Eng. Radiat. Sci.* **8**, 031702 (2022). <https://doi.org/10.1115/1.4051538>
16. A. del Corno, S. Morandi, F. Parozzi et al., Experiments on aerosol removal by high-pressure water spray. *Nucl. Eng. Des.* **311**, 28–34 (2017). <https://doi.org/10.1016/j.nucengdes.2016.06.043>
  17. H.Y. Yu, H.F. Gu, Z.N. Sun et al., Study on the influence of droplet agglomeration on the removal of aerosol by spray system. *Prog. Nucl. Energy* **140**, 103903 (2021). <https://doi.org/10.1016/j.pnucene.2021.103903>
  18. S.M. Greenfield, Rain Scavenging of radioactive particulate matter from the atmosphere. *J. Atmos. Sci.* **14**, 115–125 (1957). [https://doi.org/10.1175/1520-0469\(1957\)014%3c0115:RSORPM%3e2.0.CO;2](https://doi.org/10.1175/1520-0469(1957)014%3c0115:RSORPM%3e2.0.CO;2)
  19. H. Liang, Q. Zhou, N. Erkan et al., Improvement of aerosol spray scavenging efficiency with water mist. *J. Aerosol Sci.* **153**, 105697 (2021). <https://doi.org/10.1016/j.jaerosci.2020.105697>
  20. H. Liang, Q. Zhou, N. Erkan et al., Effect of spray properties on aerosol scavenging efficiency with water mist. *Aerosol Sci. Technol.* **56**, 29–45 (2021). <https://doi.org/10.1080/02786826.2021.1966377>
  21. B. Blaisot, M. Pellegrini, H. Liang et al. *Study of the aerosol dispersion control by a spray system during Fukushima Daiichi fuel debris retrieval*, in *Paper presented at the 19th International Topical Meeting on Nuclear Reactor Thermal Hydraulics (NURETH-19)*, Brussels, Belgium, March 6–11 (2022)
  22. E. Porcheron, Y. Leblois, T. Gelain et al. *Study of spray scrubbing as mitigation means against aerosol dispersion during the Fukushima Dai-ichi fuel debris retrieval*, in *Paper presented at the 27th International Conference on Nuclear Engineering (ICONE27)*, Tsukuba, Japan, May 19–24 (2019). <https://doi.org/10.1299/jsmeiconc.2019.27.1234>
  23. A.K. Sharma, E. Ozdemir, R. Xu et al., *Spray Characterization using Shadowgraphy for Spray Nozzles*, in *Paper presented at the 11th International Conference on Multiphase Flow (ICMF 2023)*, Kobe, Japan, April 2–7 (2023)
  24. L. Mölter, P. Keßler, Partikelgrößen- und partikelanzahlbestimmung in der außenluft mit einem neuen optischen aerosolspektrometer (Determination of the particle size and particle number in the outside air by means of a new optical aerosol spectrometer). *Gefahrstoffe Reinhalt. Luft* **64**, 439–447 (2004)
  25. H. Liang, *Development of an effective spray system for aerosol dispersion control during the decommissioning of Fukushima Daiichi nuclear power plant*, Dissertation (The University of Tokyo, Tokyo, 2020)
  26. F. Hähner, G. Dau, F. Ebert, Inertial impaction of aerosol particles on single and multiple spherical targets. *Chem. Eng. Technol.* **17**, 88–94 (1994). <https://doi.org/10.1002/ceat.270170204>
  27. D.A. Powers and S.B. Burson, *A Simplified Model of Aerosol Removal by Containment Sprays*, Sandia National Laboratories, NUREG/CR-5966, SAND92-2689 (1993). <https://doi.org/10.2172/6503368>
  28. W.G.N. Slinn, Precipitation scavenging of aerosol particles. *Geophys. Res. Lett.* **3**, 21–22 (1976). <https://doi.org/10.1029/GL003i001p00021>
  29. H. Liang, N. Erkan, V. Solans et al., Numerical simulation and validation of aerosol particle removal by water spray droplets with OpenFOAM during the Fukushima Daiichi fuel debris retrieval. *Front. Energy Res.* **8**, 102 (2020). <https://doi.org/10.3389/fenrg.2020.00102>